The Divergence Fields Associated with Time-Dependent Jet Streams

BARUCH ZIV

Department of Atmospheric Sciences, Institute of Earth Sciences, The Hebrew University of Jerusalem, Jerusalem, Israel, and The Open University of Israel, Tel Aviv, Israel

NATHAN PALDOR

Department of Atmospheric Sciences, Institute of Earth Sciences, The Hebrew University of Jerusalem, Jerusalem, Israel

(Manuscript received 31 March 1997, in final form 10 August 1998)

ABSTRACT

This study examines the effect of temporal variations in either location or structure of both straight and curved jets on their associated divergence patterns. For each of these jets the time-dependent geopotential height field is prescribed analytically, from which the geostrophic and ageostrophic wind fields are extracted. The divergence fields are calculated separately for the steady state (which was commonly assumed in studies on this subject) and for the following time-dependent cases: progressing, retrograding, intensifying, and weakening jets. In this study, the ''intensification'' of a straight jet implies an increase in the wind speed while in the case of a curved jet the intensification refers to an increase in the meandering aspect, that is, amplitude divided by wavelength.

The dominant divergence pattern of a straight jet consists of a quadrupole structure of four divergence/convergence centers, and in the case of a curved jet the pattern consists of a periodic chain of centers (of alternating signs) located along the jet axis at the inflection points. In progressing and retrograding straight and curved jets, the divergence patterns remain unaltered compared with those of the steady state, but the amplitude decreases in the former and increases in the latter. For an intensifying straight jet, the divergence patterns increase at the entrance region and weaken at the exit, while at the same time being slightly shifted downstream. The reverse holds for the weakening straight jet. The changes in the meandering aspect of a curved jet are accompanied by an intensification of the divergence patterns in both the intensifying and weakening jets. These are accompanied by a shift in their location relative to the jet: downstream for the intensifying jet and upstream for the weakening one.

These findings point to the effect of time dependence on the cyclogenesis associated with jet streams and on feedback mechanisms there. For each of the cases considered here, the authors demonstrate that the divergence patterns indicate a negative feedback, which tends to suppress the prescribed temporal change.

1. Introduction

The upper-level 2D divergence field is strongly related to surface cyclogenesis and midtropospheric vertical motion (e.g., Uccellini et al. 1985; Uccellini and Kocin 1987; Keyser and Shapiro 1986, KS86 hereafter). This is contributed mainly by the ageostrophic wind component (Holton 1992). Using a natural coordinate system, it can be shown (see appendix A) that the divergence magnitude can be expanded as a polynomial in the wind speed, so that the divergence centers are expected to be found near jet streams. Both Palmen and Newton (1969, PN69 hereafter) and Shapiro and Kennedy (1981) have shown that this hypothesis is supported by observations and that the ageostrophic wind component in the vicinity of jets attains the same order of magnitude as that of its geostrophic counterpart.

Studies of the ageostrophic circulations associated with jets distinguish between straight jets (e.g., KS86; Nakamura 1993) and curved ones (e.g., KS86; Cammas and Ramond 1989). The schematic representation of the ageostrophic motions and the associated divergence patterns that typify both jets are shown in Figs. 1a,b [reproduced from Shapiro and Kennedy (1981)].

Divergence patterns for a straight jet similar to those shown in Fig. 1a were derived by KS86 from the Sawyer–Eliassen equations for the case where thermal advection and pressure gradient are constant. Similar patterns were also obtained from the steady-state approximated vorticity equation by Uccellini and Kocin (1987), who noted the existence of positive and negative vorticity advection regions (PVA and NVA, respectively, in Fig. 2).

These features are explained conceptually (e.g., Bjerknes 1951) by the rapid variations in the pressure gradient force experienced by the air parcels upon en-

Corresponding author address: Dr. Nathan Paldor, Department of Atmospheric Sciences, Institute of Earth Sciences, The Hebrew University of Jerusalem, Givat Ram, Jerusalem 91904, Israel.
E-mail: paldor@vms.huji.ac.il

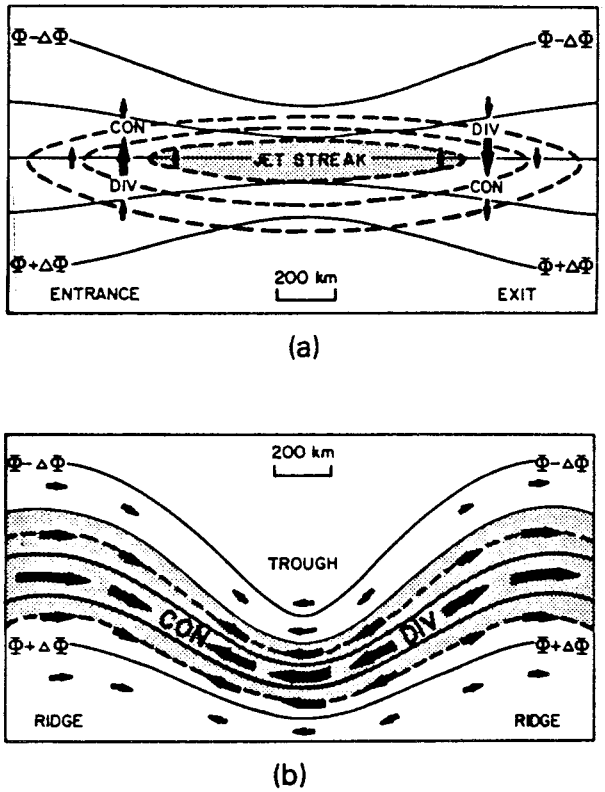

FIG. 1. A schematic representation of the ageostrophic motion (heavy arrows) and associated patterns of convergence (CON) and divergence (DIV) in the vicinity of (a) a straight jet and (b) an along-stream uniform curved jet. Adapted from Shapiro and Kennedy (1981).

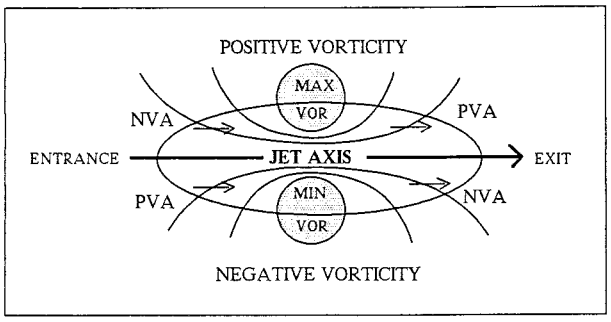

FIG. 2. Divergence patterns associated with positive/negative shear vorticity (PVA/NVA) in the vicinity of a straight jet, following Uccellini and Kocin (1987).

tering or leaving the jet. In the entrance region, for example, this force increases and diverts the air parcels to the left of their geostrophic direction, causing convergence (divergence) to the left (right) of the jet axis (CON/DIV in Fig. 1a). Observational evidence (e.g., Cammas and Ramond 1989) support the above expectations.

Nakamura (1993) analyzed the 10 years of National Meteorological Center (now the National Centers for Environmental Prediction) data of the winter Asian jet and found a somewhat different divergence pattern. The analysis indicates that the common quadrupole is superposed upon an east–west-oriented dipole, such that the convergence center to the left of the jet entrance dominates the entrance region, whereas the divergence pattern to the left of the jet exit dominates the exit region. Nakamura attributed this additional dipole structure to the contribution of vorticity advection by the ageostrophic transverse wind. The north–south vorticity gradient is pronounced along a zonal straight jet due to the combined contribution of both the β effect and the wind shear. Therefore, the southern ageostrophic wind across the jet entrance contributes negative vorticity advection there, so as to enhance the convergence there. The reverse holds for the jet exit.

The curved jet was studied by Bjerknes and Holmboe (1944) and by Newton and Trevisan (1984), who both adopted the vorticity equation approach. They showed that the positive vorticity advection has a maximum ahead of the upper-level trough, right above the location of the divergence center. Similar results were obtained in KS86 by analyzing the divergence operator in the natural coordinate system for a curved jet with an along-contour uniform speed. Many other references of studies dealing with a steady curved jet are given in atmospheric dynamics textbooks, such as PN69, Dutton (1976), and Holton (1992).

PN69 showed that the magnitude of the divergence patterns, when averaged between successive ridge/trough lines, decreases linearly with the phase speed of the wave in which the jet is embedded. This implies that the magnitude of the divergence patterns associated with a progressing curved jet is smaller than that associated with a stationary jet (hence, an increase in the divergence is expected for a retrograding jet). This consideration has motivated us to study, more comprehensively, the divergence patterns in cases when the jet is time dependent, whether in location or in structure.

In this study we assess the effects of various types of temporal variations on the divergence patterns associated with straight and curved jets. Jet streams are commonly described by their isotach structure, which can either simply move zonally intact or vary in structure, reflecting an intensification or weakening. The latter can be expressed by the changes in wind speed for the straight jet and the degree of meandering for the curved one.

The analysis of the divergence structure is carried out for 10 different idealized cases—5 for each of the straight and curved jets. These five cases include steady (which serves as a reference case), progressing, retrograding, intensifying, and weakening jets. The methodology adopted is the same for all cases: First, the geopotential height at the level of maximum wind is prescribed (including the time-dependent factor appli-

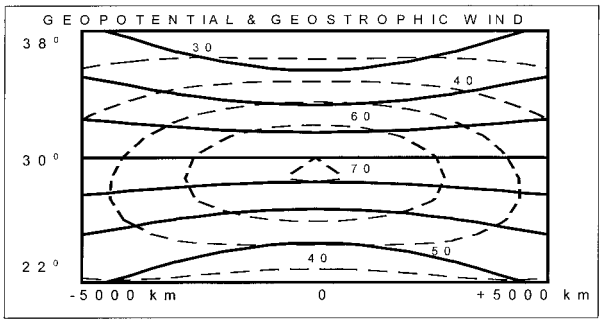

FIG. 3. Horizontal cross section (abscissa—zonal distance, in km; ordinate—latitude, in degrees) of geopotential height (solid) and isotachs of the geostrophic wind (m s^{-1}, dashed) for a straight jet, calculated from Eqs. (1)–(3).

cable for the particular case). Second, the geostrophic wind is extracted. Third, the ageostrophic wind component is derived from the acceleration (or turning) of the geostrophic wind. Last, the divergence field is calculated from the wind field.

The paper is organized as follows: Section 2 deals with the divergence patterns associated with a straight jet. Section 3 discusses the divergence along the axis of a curved jet with a uniform wind speed and extends the results into a 2D framework. Section 4 discusses the implications of the results to the feedback mechanisms that affect the jets, and section 5 summarizes the results and their implications and outlines suggestions for further research.

2. Straight jet

a. Structure

The geopotential height field Φ for the straight jet follows the classic description of the Bickley jet (Peng and Williams 1986; Dutkiewicz and Paldor 1994):

$$\Phi = \Phi_0 + \Phi_1 \tanh\left(\frac{y_0 - y}{\Delta y}\right), \tag{1}$$

where Φ_0 is the geopotential along the jet axis, located at $y = y_0$, and $\Delta y(x, t)$ is the width of the jet, given by

$$\Delta y = \Delta y_0(1 - \Delta_1 t)\frac{2}{1 + \exp\left[-\left(\frac{x - ct}{\Delta x}\right)^2\right]}, \tag{2}$$

where Δy_0 is the jet width at the longitude of maximum wind at $t = 0$, Δ_1 is the so-called amplification factor, c is the phase speed, and Δx is half of the jet length. The geopotential field is shown in Fig. 3 (solid). These widths govern the wind speed along the jet axis. The movement and amplification of the jet are determined by the phase speed and the amplification factor, respectively.

The x and y components of the geostrophic wind (u_g and v_g, respectively) are extracted from the geopotential field using the relations (e.g., Holton 1992)

$$u_g = \frac{-1}{f}\frac{\partial \Phi}{\partial y}; \qquad v_g = \frac{1}{f}\frac{\partial \Phi}{\partial x}, \tag{3}$$

where f is Coriolis parameter. The y variation of the wind speed on an f plane of this Bickley jet follows from Eq. (1):

$$V = V_{\max}\,\mathrm{sech}^2\frac{(y - y_0)}{\Delta y}, \tag{4}$$

where V and $V_{\max}$ [$=\Phi_1/(f_0\Delta y)$] are the wind speed and the maximum wind speed at a given longitude, respectively and Δy is defined in Eq. (2). The geopotential field of Eqs. (1)–(2) and the associated geostrophic wind speed of Eq. (3) are shown in Fig. 3. This wind field differs slightly from that given in Eq. (4) due to the variation of Coriolis parameter with y. Since the straight jet studied here describes the subtropical jet (e.g., Nakamura 1993), y_0 was set to correspond to 30° latitude. The amplitude of the width, Δy_2, and length of the jet were set to 900 and 9000 km, respectively, and the geopotential field was adjusted to yield a maximum wind speed of 70 m s^{-1}.

The ageostrophic y component v_a is derived from the geostrophic wind field, assuming the so-called cross-front geostrophy (e.g., KS86):

$$v_a = \frac{1}{f}\frac{du}{dt} \cong \frac{1}{f}\left[\frac{\partial u_g}{\partial t} + u_g\frac{\partial u_g}{\partial x} + (v_g + v_a)\frac{\partial u_g}{\partial y}\right], \tag{5}$$

from which v_a can be solved to yield

$$v_a \cong \frac{1}{f}\frac{1}{\left(1 - \frac{1}{f}\frac{\partial u_g}{\partial y}\right)^{-1}}\left(\frac{\partial u_g}{\partial t} + u_g\frac{\partial u_g}{\partial x} + v_g\frac{\partial u_g}{\partial y}\right). \tag{6}$$

The inclusion of v_a in the advection term on the rhs of (5) leads to a more accurate approximation than that implied by the quasigeostrophic one. This is, indeed, the main contribution to the different scenario envisioned by Nakamura (1993) as compared with the quasigeostrophic approach in Uccellini and Kocin (1987).

The contribution of the ageostrophic x component u_a to v_a is ignored here (as well as in previous ones) since the assumed zonal orientation of the straight jet implies that v_a and u_a *should* be considered as the transverse and along-stream ageostrophic wind components, respectively. Therefore, the former is proportional to the wind acceleration, which is significant in a straight jet, whereas the latter is proportional to the flow curvature (gradient effect), assumed negligible here (Fig. 3). Numerical calculation of $(-1/f)(\partial v/\partial x)u_g$, which approximates u_a, verified indeed that u_a is 1–2 orders of magnitudes smaller than u_g.

The contribution of u_a to the divergence field may be estimated from the relative magnitude of terms in the expression for the divergence of the ageostrophic wind,

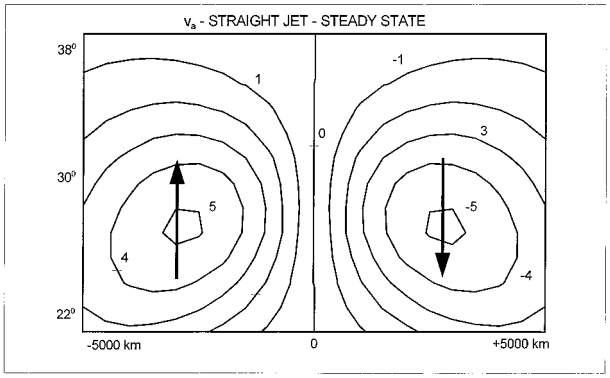

FIG. 4. Meridional ageostrophic velocity, (in m s^{-1}), for the steady-state straight jet shown in Fig. 3.

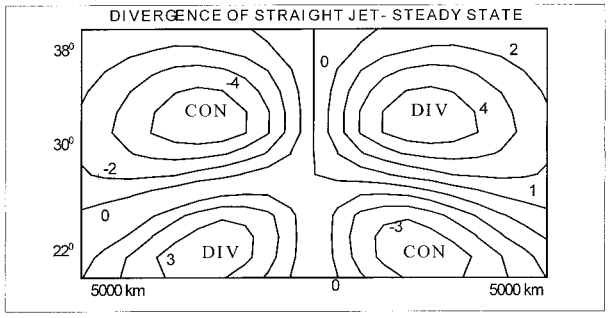

FIG. 5. Contours of divergence field (in 10^{-6} s^{-1}, solid) of a steady-state straight jet (Fig. 3).

$$\nabla \cdot \mathbf{V}_a = \frac{\partial u_a}{\partial x} + \frac{\partial v_a}{\partial y}, \tag{7}$$

as follows. The rhs of (7) is approximated by $[u_a]/[\Delta x] + [v_a]/[\Delta y]$, where each square bracket denotes the respective characteristic value. Even when $[u_a]$ is about half of $[v_a]$, $[\Delta x]$ is at least 1 order of magnitude larger than $[\Delta y]$, which implies that the first term on the rhs of (7), that is, the contribution of u_a to the divergence, is much smaller (by at least a factor of 20) than the second term. Thus, the divergence fields for various straight jets are calculated from both the geostrophic wind components and the ageostrophic v component, while the ageostrophic u component is neglected.

b. Steady-state case

The steady-state condition is obtained by setting both the phase speed and the amplification factor in Eq. (2) to zero. The ageostrophic wind field for this case is shown in Fig. 4. It consists of two similar and opposite meridional flow segments with maximum speed of 6 m s^{-1}. The associated divergence field, shown in Fig. 5, has four extrema with magnitudes of over $+3 \times 10^{-6}$ s^{-1} and $+4 \times 10^{-6}$ s^{-1} (divergence) to the right of the entrance region and to the left of the jet exit, respectively, and -4×10^{-6} s^{-1} and -3×10^{-6} s^{-1} (convergence) to the left of the entrance and to the right of the exit of the jet, respectively. This is similar to that seen in Figs. 1 and 2, but the extrema to the left (north) of the jet axis are somewhat larger, as found by Nakamura (1993); see discussion in appendix B.

c. Time-varying cases

For moving jets, the amplification factor Δ_1 was set to zero and the phase speed c, in Eq. (2), to $+15$ m s^{-1}, (-15 m s^{-1}) corresponding to a progressing (retrograding) jet. The respective divergence fields are shown in Figs. 6a,b from which it is evident that the structure and location of the centers are essentially the same as those of the steady jet but their magnitudes are smaller (larger) for the progressing (retrogressing) jet. For the progressing jet the magnitudes of the centers to the left of the jet axis are reduced to 3×10^{-6} s^{-1} while those located at the right side are reduced to only 1×10^{-6} s^{-1}. For the retrograding jet the magnitude of all divergence centers increases to about 6×10^{-6} s^{-1}.

In the case of jets with varying intensity, the phase speed was set to zero, and Δ_1, in Eq. (2), was set to $+\frac{1}{6}$ day^{-1} ($-\frac{1}{6}$ day^{-1}) for intensifying (weakening) jet. The structure of the divergence field (Figs. 6c,d) is similar to that of the steady jet, except for a pronounced asymmetry between the entrance and the exit regions of the jet. For the intensifying jet, the extreme values of the centers located at the entrance region are significantly larger compared with those of the steady jet, whereas the extreme values of those located at the jet exit are significantly smaller. The relative change in the magnitudes of the centers located to the left of the jet axis is about 50%, whereas the relative change in the values of those located to the right is on the order of 100%, so the convergence center at the right of the exit region nearly disappears. The asymmetry between the exit and the entrance regions reverses in the weakening jet, and the asymmetry with respect to the jet axis is similar.

In both time-dependent cases the variation in the intensity of the divergence centers with respect to the steady jet is significantly larger for those located to the right (south) of the jet axis than those located to its left (north).

d. Qualitative considerations

The magnitude and location of the divergence centers can be related to the ageostrophic wind field. It turns out from Eqs. (5) and (6) that the ageostrophic wind speed is proportional to the acceleration experienced by air parcels as they move through the jet. This acceleration may be estimated by the rate at which air parcels cross the isotachs. Its magnitude at a certain location is inversely proportional to the distance between successive intersections of the isotachs with the streamline of

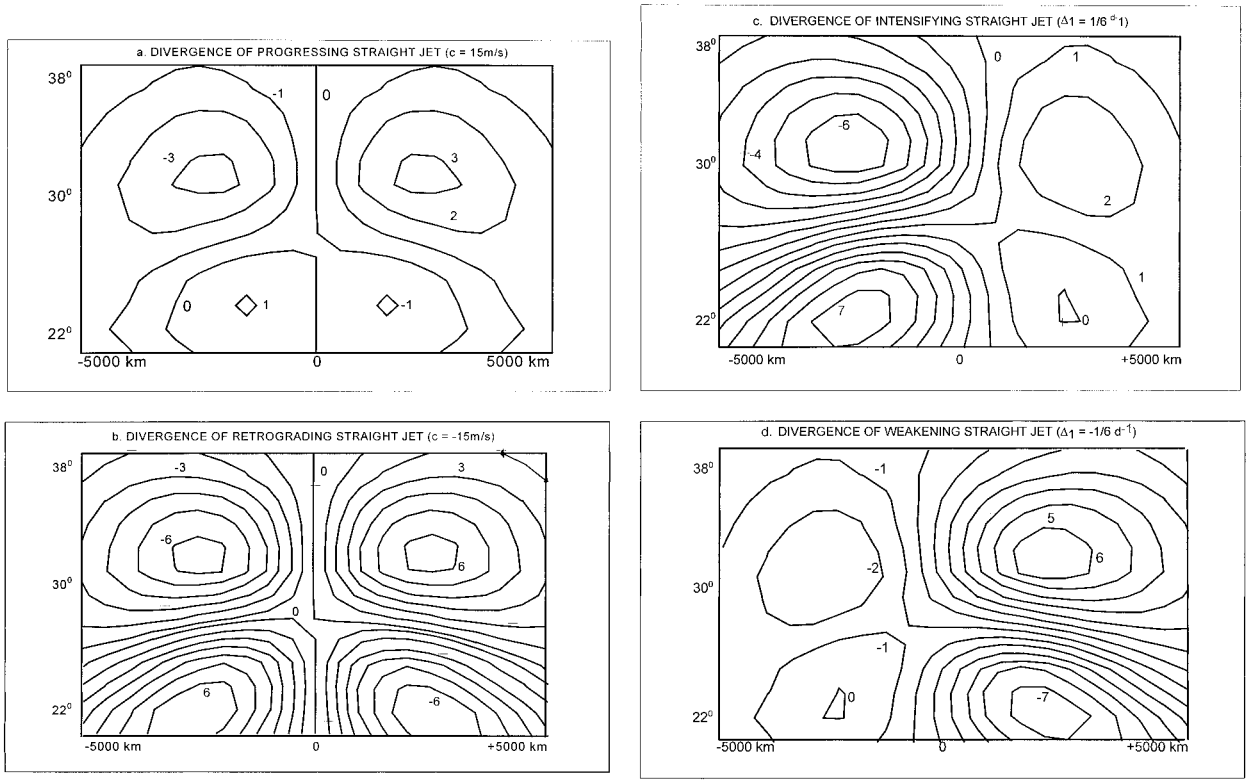

FIG. 6. Divergence field (in 10^{-6} s^{-1}, solid) for (a) progressing jet ($c = 15$ m s^{-1}), (b) retrogressing jet ($c = -15$ m s^{-1}), (c) intensifying jet and ($\Delta_1 = 0.16$ day^{-1}), and (d) weakening jet ($\Delta_1 = -0.16$ day^{-1}).

the geostrophic wind, that is, the geopotential contours. The largest acceleration is, therefore, expected to be found along the axis of the jet at the entrance and exit regions (Fig. 3). Equation (7), together with Figs. 4 and 5, suggests that the divergence centers appear in pairs located at both ends of each of the ageostrophic flow segments and that the magnitude of the divergence extrema is proportional to the maximum ageostrophic wind speed.

The considerations described above hold for steady-state conditions. For time-dependent conditions, we have to consider in addition the movement of the isotachs themselves, which locally modifies the rate at which air parcels, which now move in a field of moving isotachs, cross them.

When an air parcel enters the jet while the isotachs there retrograde (move against it), its acceleration increases, so that the resulting ageostrophic wind increases, along with the intensity of the associated divergence centers. On the other hand, a progression of the isotachs at the entrance region reduces the acceleration of air parcels and, hence, by the same argument, the intensity of the associated divergence centers is reduced. When an air parcel leaves the jet, the retrogression of the isotachs enhances its acceleration (and therefore the speed of the associated ageostrophic flow segment), and, hence, the intensity of the associated divergence centers increases accordingly. A progression of the isotachs at the exit region results in a decrease of the intensity of the divergence centers there. This qualitative reasoning supports the quantitative differences between the four panels shown in Fig. 6 and that of Fig. 5, as follows.

When the jet moves downstream, the isotachs progress in both the entrance and exit regions (Fig. 7a), thus reducing the divergence intensity in both regions. The opposite (i.e., an increase in the divergence intensity at both exit and entrance regions) holds for a retrogressing jet (Fig. 7b), due to the retrogression of the isotachs in both regions. These conclusions agree with our results (cf. Fig. 5 with Figs. 6a,b).

Considering the variations in the jet's intensity, an intensification (weakening) of the jet is accompanied by an expansion (shrinking) of the isotachs (Figs. 7c,d). Consider first an intensifying jet: the isotachs retrograde at the entrance as part of their expansion and progress at the exit (Fig. 7c). As discussed above, these relative motions of the isotachs enhance the air parcel's acceleration (and the divergence magnitude) at the jet's entrance and reduce it at its exit, as seen in Fig. 6c. The link between the parcel's acceleration and the divergence is the ageostrophic wind, the changes of which are shown in Fig. 8 in both regions of the intensifying jet. A comparison with the corresponding changes in the steady jet (Fig. 4) supports the hypothesized inten-

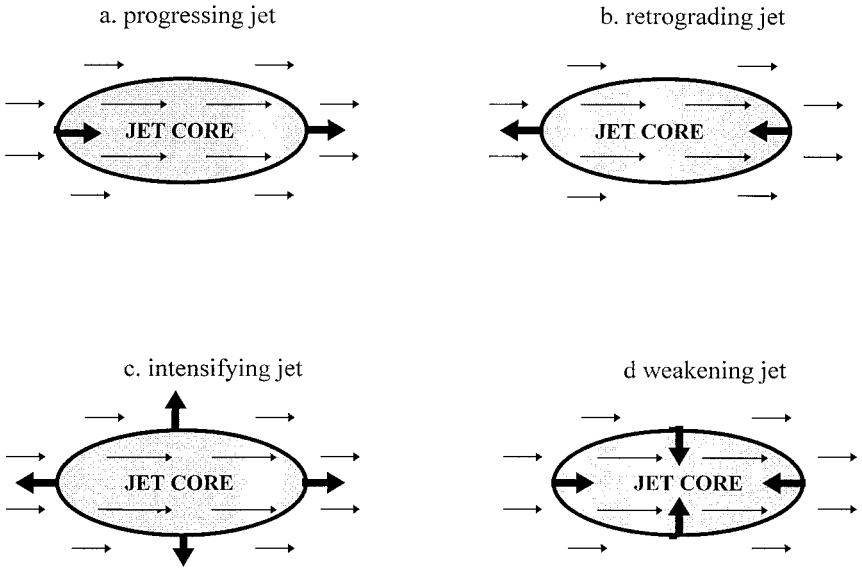

FIG. 7. Schematics of the four types of time-dependent straight jets (Fig. 6). Heavy ellipses represent the isotach of 60 m s^{-1}, the thin arrows represent the wind vectors, and the heavy arrows denote the movement of the isotach.

sification of the flow segment across the jet entrance and its weakening at the exit region. For similar arguments, these changes reverse in a weakening jet, in agreement with our quantitative results shown in Fig. 6d. Furthermore, the gradient of the wind speed at the jet center vanishes, so the air parcels are accelerated there due only to the temporal change in the wind speed. Thus, at the center of intensifying jets an acceleration of air parcels is anticipated following the intensification of the jet while in weakening jets deceleration is expected there. This implies that the wind at the center of a jet experiences similar conditions to those at the entrance region for intensifying jet, and similar to those in the exit region for a weakening jet. Therefore, there is an extension of the ageostrophic wind pattern toward the jet's center from the entrance (exit) region in an intensifying (weakening) jet, in accordance with the respective shifts found in the ageostrophic wind patterns shown in Fig. 8.

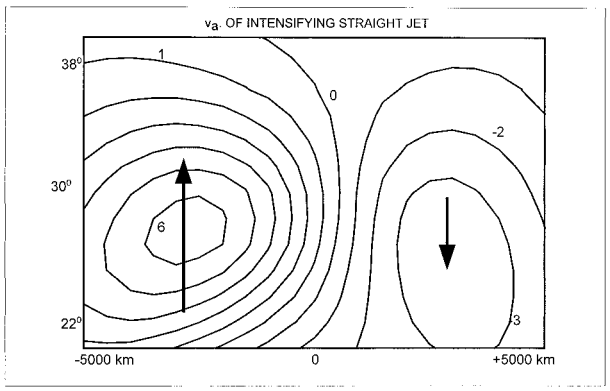

FIG. 8. Same as Fig. 4 but for the intensifying straight jet shown in Fig. 6c.

The above discussion refers to the implications of the acceleration of air parcels, when they cross the jet. The factor $1/f$, which appears on the rhs of Eq. (5), explains why the variation in the magnitude of the centers located to the south of the jet axis is significantly larger than that found for the centers located to the north of the axis.

3. Curved jet

When discussing the divergence field associated with a curved jet, KS86 and PN69 both consider only jets with a uniform wind speed, where a gradient balance prevails. To simplify the exposition in the more general case studied here, we start with a 1D analysis of the divergence along the jet axis only (section 3a), assuming a uniform along-contour speed there, and defer the more general 2D analysis to the (section 3b).

Following PN69, the angle α between the streamline of the jet axis and the east direction (to the left) and is assumed to vary with x and t according to

$$\alpha \equiv \frac{dy}{dx} = \frac{v}{u} = A\cos[k(x - ct)];$$
$$A \equiv A_0 + A_1 t, \tag{8}$$

where u and v are the components of the total wind, A is the meandering aspect that contains a constant factor A_0, taken as 0.25, and an amplification factor A_1, and k is the wavenumber, corresponding to wavelength L of 6000 km. The latitude of the jet axis y_0 obtains by integrating Eq. (8) with respect to x, that is,

$$y_0 = A\frac{\sin[k(x - ct)]}{k} + y_{00}, \tag{9}$$

where y_{00} is the constant of integration, which determines the average value of y_0. Since the curved jet is typically encountered in midlatitudes (e.g., PN69), y_{00} was set to 45° latitude.

a. The 1D approach

This part deals with the divergence of the wind along the jet axis, assuming a uniform wind speed there. The computations were carried out assuming a gradient balance. The necessary condition for a gradient balance to prevail is that the total time derivative of the wind speed, dV/dt, is zero. For a steady jet the streamlines coincide with the trajectories; hence the assumed uniform wind speed along the jet axis implies that the air parcels moving there maintain a constant speed, so the gradient balance does indeed hold. By contrast, in a time-dependent jet, where the streamlines do not coincide with the trajectories, air parcels may cross the axis, so their speed may change. However, at the time of crossing the jet axis, where the wind speed is maximum, the instantaneous total time derivative of their speed is zero. Hence, the necessary condition for a gradient balance to exist is satisfied along the jet axis even in time-dependent jets.

The isobaric divergence operator $\nabla_p \cdot \mathbf{V}_{gr}$ for a uniform, along-contour gradient wind is (see, e.g., KS86)

$$\nabla_p \cdot \mathbf{V}_{gr} = -\left(1 - \frac{K_t V_{gr}}{f}\right)^{-1}\left[\frac{\beta}{f}v_{gr} + \frac{V_{gr}}{f}(\mathbf{V}_{gr} \cdot \nabla_p K_t)\right], \tag{10}$$

where V_{gr} is the speed of the gradient wind, chosen to be 70 m s^{-1}, v_{gr} is the y component of the gradient wind, β is $\partial f/\partial y$, and K_t is the trajectory curvature. This trajectory curvature for a general flow of speed V is given in natural coordinates by

$$K_t \equiv \frac{d\alpha}{ds} = \frac{1}{\sec\alpha}\frac{\partial\alpha}{\partial x} + \frac{1}{V}\frac{\partial\alpha}{\partial t} \equiv K_s + \frac{1}{V}\frac{\partial\alpha}{\partial t} \tag{11}$$

(Dutton 1976), where ds is an infinitesimal increment along the wind direction and K_s is the streamline curvature parameter. Equations (10) and (11) imply that the relationship between the speed of the gradient wind and that of the geostrophic wind depends on both the geometry of the wind field and its time evolution.

Figure 9 shows the calculated divergence of the gradient wind along the jet axis, following Eqs. (8), (10), and (11) for the five cases. For the steady-state case (A_1 and c both vanish) the divergence has a sinusoidal dependence on x with a phase relation to the geometry of the jet axis, in agreement with Fig. 1. The divergence pattern for the progressing or retrogressing waves ($c = +15$ m s^{-1} and $c = -15$ m s^{-1}, respectively) has the same x variation as in the steady-state case, except for

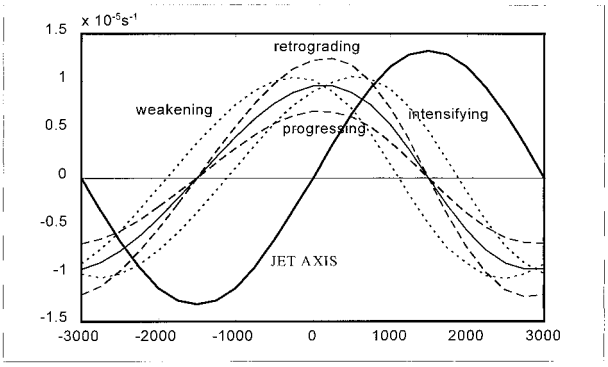

FIG. 9. Variation of the divergence of the gradient wind with x along the axis of the curved jet with a uniform speed of 70 m s^{-1} for the steady state (thin solid), progressing ($c = 15$ m s^{-1}), retrogressing ($c = -15$ m s^{-1}, both dashed), intensifying ($A_1 = 0.5$ day^{-1}), and weakening ($A_1 = 0.5$ day^{-1}, both dotted) cases. The heavy solid line represents the geometry of the jet.

a decrease (increase) in the amplitude for the progressing (retrogressing) wave, in agreement with PN69. The intensifying and weakening jets ($A_1 = +0.25$ day^{-1} and $A_1 = -0.25$ day^{-1}, respectively) both yield higher amplitudes than the steady-state case, and a significant phase shift, of about 1/10 wavelength, downstream for the intensifying jet and upstream for the weakening jet.

These numerical results may be interpreted by approximating Eq. (10). Applying $f = f_0 = 10^{-4}$ so $\beta = 0$ yields

$$\nabla_p \cdot \mathbf{V}_{gr} \cong -\frac{V^2}{f_0}\frac{\partial K_t}{\partial s} = -\frac{V^2\cos\alpha}{f_0}\frac{\partial K_t}{\partial x}, \tag{12}$$

implying that the divergence is dominated by the spatial variation of the flow curvature. Substituting Eq. (8) in Eq. (11) yields

$$K_t = -kA\cos\{A\cos[k(x - ct)]\}\sin[k(x - ct)] + \frac{1}{V}\{A_1\cos[k(x - ct)] + kcA\sin[k(x - ct)]\}, \tag{13}$$

and when Eqs. (8) and (13) are substituted in Eq. (12), the result is

$$\nabla_p \cdot \mathbf{V}_{gr} \cong k^2\frac{V_{gr}^2}{f_0}\cos\alpha \times\left\{\sin\alpha A^2\sin^2[k(x - ct)] + \alpha\cos\alpha + \frac{1}{V_{gr}}\left\{-\alpha c + A_1\frac{\sin[k(x - ct)]}{k}\right\}\right\}. \tag{14}$$

The first two terms inside the outermost brackets on the rhs of (14) reflect the divergence of a steady jet ($c = 0$, $A_1 = 0$), and the next two terms reflect the contributions due to time variations: the third term is related to the wave motion while the fourth term is due to the temporal variation of the meandering aspect.

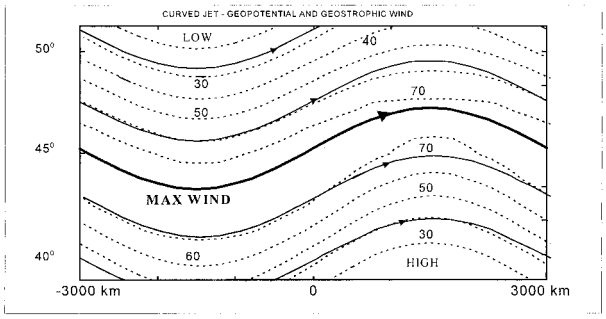

FIG. 10. Geopotential height (solid) and geostrophic wind speed of a curved jet in the steady state calculated from Eqs. (17) and (3). Isotachs (dashed) are drawn in units of m s^{-1} with a 10 m s^{-1} interval. Axes are as in Fig. 3.

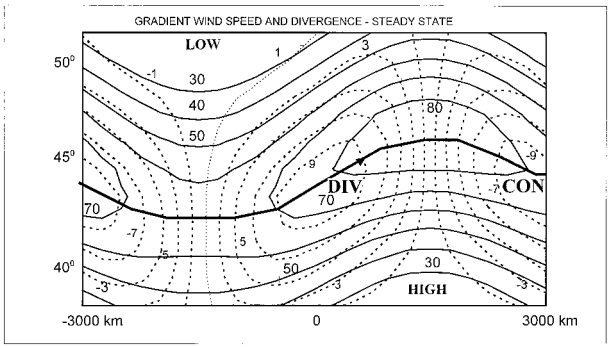

FIG. 11. Gradient wind for the case shown in Fig. 10 calculated from Eq. (16). Isotachs (solid, 10 m s^{-1} interval) and isolines of divergence (dashed, in 10^{-6} s^{-1} with a 2.0 interval). Regions of convergence and divergence are designated CON and DIV, respectively. HIGH and LOW denote geopotential height. The thick solid curve represents the jet axis.

By our choice of parameters the meandering aspect is smaller than 1 for times on the order of 1 day. Hence, for short enough times, the parameter A and, by virtue of Eq. (8), α, too, can be assumed small. So, neglecting higher-order terms in A and α we get

$$\nabla_p \cdot \mathbf{V}_{gr} \cong \frac{V_{gr}^2 k^2}{f}\left\{A\cos[k(x - ct)] + \frac{1}{V_{gr}}\left\{-A\cos[k(x - ct)]c + \frac{A_1}{k}\sin[k(x - ct)]\right\}\right\}. \quad (15)$$

The first term in (15) is in phase with α, and hence with the v wind component (see Fig. 9). The second term is 180° out of phase with α, implying that the divergence patterns are unaltered by the wave motion, but their amplitude decreases when the wave progresses (positive c) and increases when it retrogrades (negative c). The third term is proportional to $\sin[k(x - ct)]$, so its contribution lags behind that of the other terms by 90° in the case of an intensifying jet ($A_1 > 0$) and precedes it in the case of a weakening jet ($A_1 < 0$). This explains the phase shift in the divergence patterns found in all four cases. The magnitude of the divergence extrema is larger than that of the steady-state case for the cases in which $A_1 \neq 0$. This is a general result of combined sinusoidal variables, being 90° out of phase (appendix C).

b. The 2D approach

In this section the curved jet is studied over a 2D domain with 6000 km in the x direction (one wavelength) and 1500 km in the y direction (Fig. 10). The analysis in this section covers both sides of the jet axis, where the streamlines are parallel to each other and they all have the same geometry and time dependence as in the previous section. Unlike the 1D case, simple and exact results are not available here, so only numerical results of the 2D divergence operator are presented. The geopotential field was designed to yield y variation of the wind speed, following the Bickley jet (1), that is,

$$\Phi = \Phi_0 + \Phi_1 \tanh\left(\frac{y_0 - y}{\Delta y}\right), \quad (16)$$

where y_0 is given by (9), and the jet width Δy is 700 km and is uniform along the jet. The meandering aspect is 0.25 in this case, too. The constant Φ_1 and the jet width are set so as to yield a maximum wind around 80 m s^{-1}. The geostrophic wind field, extracted from (16) using (3), is shown in Fig. 10. The variation of the geostrophic wind speed along the jet axis is due only to the variation of the Coriolis parameter with y.

Here, a gradient balance provides a first-order approximation since the wind speed along the streamlines varies by no more than 10%. The gradient wind speed V_{gr} is related to that of the geostrophic wind V_g by

$$V_{gr} \cong V_g\left(1 - \frac{V_g}{f}K_t\right) \quad (17)$$

(Dutton 1976). The divergence fields were calculated numerically from the gradient wind field.

The wind speed and the divergence field for the steady-state case (i.e., both c and A_1 vanish) are shown in Fig. 11. Here, the variation of the wind speed along the jet axis is reversed with respect to its geostrophic counterpart due to the contribution of the curvature, which dominates over the β effect. The divergence centers are found along the jet axis, where the wind speed is maximum, as implied by Eqs. (10) and (12). The positive center is located downstream of the trough and the negative centers downstream of the ridge, in agreement with Figs. 9 and 1b. Both centers have the same magnitude, around 1×10^{-5} s^{-1}, that is, about four times larger than that corresponding to the geostrophic wind alone (not shown).

The parameters for a propagating jet are identical with

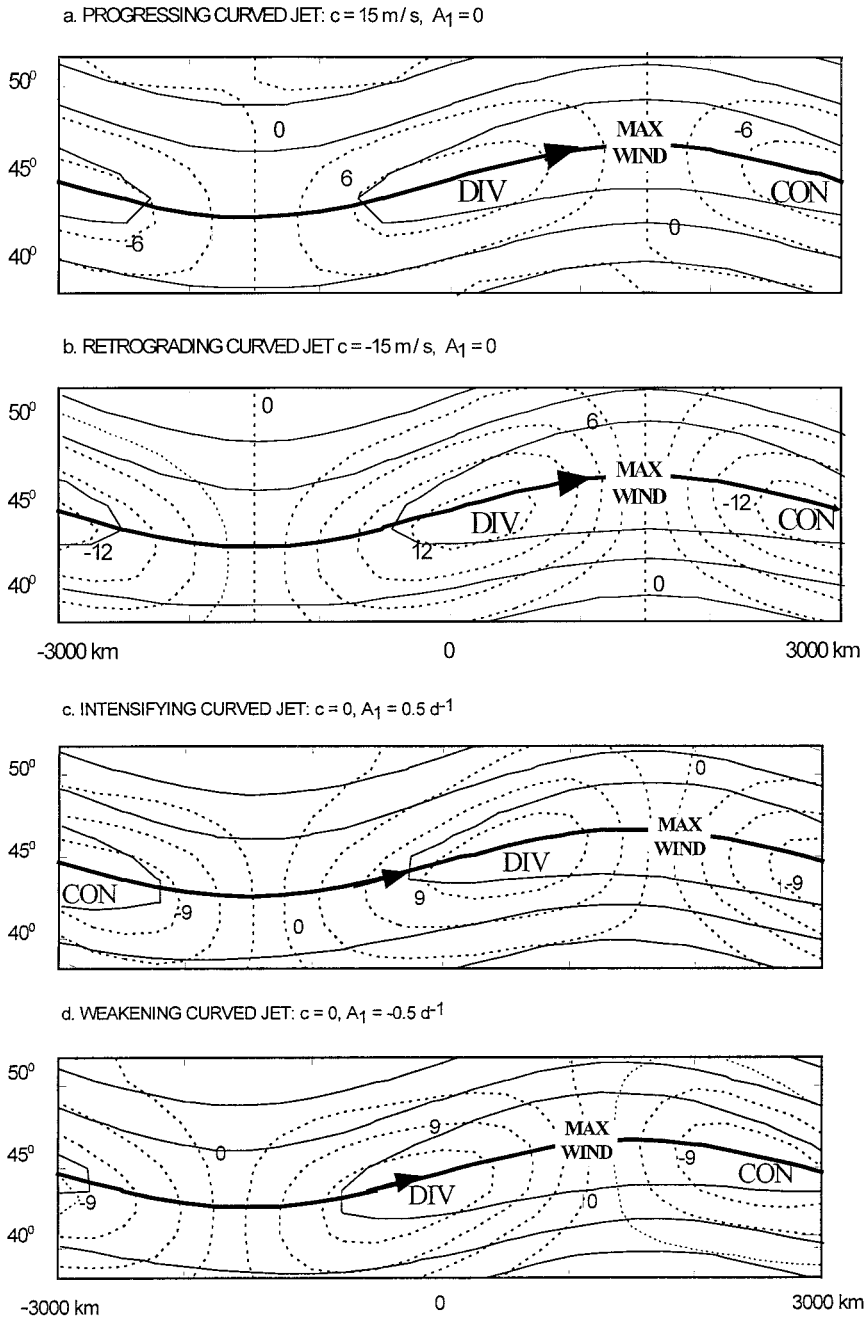

FIG. 12. Same as in Fig. 11 but for (a) progressing jet with phase speed of 15 m s^{-1}, (b) retrogressing jet with phase speed of -15 m s^{-1}, (c) intensifying jet and with amplification factor A_1 of 0.5 day^{-1}, and (d) weakening jet and with amplification factor A_1 of -0.5 day^{-1}.

those of the steady-state case, except for the phase speed c, which was set to $+15$ m s^{-1} (-15 m s^{-1}) in the case of a progressing (retrogressing) jet. The structure of the divergence field for these jets (Figs. 12a,b) are similar to that of the steady jet, except for a 20% decrease in magnitude for the progressing jet and a 30% increase for the retrograding jet, in agreement with the results obtained by the 1D approach (Fig. 9).

For jets with varying intensity, the phase speed was set to zero, but the amplification factor A_1 was set to $+0.5$ day^{-1} (-0.5 day^{-1}) for an amplifying (weakening) wave. The isotachic pattern for an amplifying wave (Fig. 12c) is shifted downstream by about 0.08 wavelength relative to that for the steady jet, and a similar shift is found in the location of the divergence centers. The magnitudes of the divergence centers are slightly (about

TABLE 1. Characteristics of time-dependent jets relative to the respective steady-state jets.

Type of time dependence	Straight jet		Curved jet	
	Intensity	Phase shift	Intensity	Phase shift
Progressing	Decrease	No	Decrease	No
Retrograding	Increase	No	Increase	No
Intensifying	Increase in entrance, decrease in exit	Not significant	Increase	Downstream, 1/10 wavelength
Weakening	Decrease in entrance, increase in exit	Not significant	Increase	Upstream, 1/10 wavelength
Comments	Changes are larger to the right (south) of the jet axis		Intensity variations are expressed as variations in the meandering aspect	

5%–10%) larger than those of the steady jet, with an increase in the magnitude of the convergence center slightly larger than that of the divergence center. The corresponding fields for a weakening wave are shown in Fig. 12d. Here, too, the isotach and divergence patterns are shifted by about 0.08 wavelength, but in this case the shift is upstream. The magnitudes of the divergence centers are also somewhat larger than those for the steady-state case, but here the increase in the magnitude of the divergence center is larger than that for the convergence centers.

In all the cases shown above the divergence centers are found along the jet axis, which reaffirms the validity of the 1D approach as, indeed, used vastly in the literature (e.g., KS86). The two approaches agree in the main results, as summarized in Table 1.

4. Discussion—Feedback consideration

a. The relation between divergence field and feedback mechanisms

The divergence field reflects the ageostrophic circulations, which constitute another (i.e., in addition to the feedback associated with the geostrophic wind) feedback mechanism for the maintenance of the jets. These ageostrophic circulations can also affect the movement of the jet itself (KS86; Holton 1992). Thus, any change in their location or intensity by any of the time dependencies studied here is expected to affect the structure and movement of the jet. The difference in the divergence intensity in the various parts of some of the jets implies then a rather complex behavior.

b. Straight jets

The starting point for the description of the effects associated with time dependencies is the delicate balance described by KS86 for the case of a steady purely confluent/diffluent straight jet. They have shown that the ageostrophic circulation counteracts the tendency of the geostrophic advection to disrupt the thermal wind balance. This tendency is manifested in the increase (decrease) of the cross-front potential temperature gradient at the confluence (diffluence) region due to advection of temperature, while at the same time decreasing (increasing) the geostrophic wind itself. This leads us to the conclusion that in the absence of ageostrophic circulations, the jet will move backward since the confluence and diffluence regions are located at the entrance and exit regions, respectively. The ageostrophic circulations, on the other hand, being direct at the entrance region and indirect at the exit region, operate in the opposite sense in both regions, so when these two effects exactly balance each other, the jet is stationary.

When time-dependent factors are introduced to the straight jet this balance is disrupted and the jet may be subject to a net forward (backward) drive when the ageostrophic circulations increase (decrease) with respect to that of the steady jet. These changes in the intensity of the ageostrophic circulations are assumed to be represented by the respective changes in the intensity of the divergence centers.

Consider the moving straight jet first. For a progressing jet, Fig. 6a shows that the divergence patterns decrease relative to the steady jet (Fig. 5) in both the exit and the entrance regions. This, in turn, implies a respective decrease of the ageostrophic circulations in both regions, so that the retarding geostrophic advection now dominates, in contrast with the prescribed progression of the jet. The retrograding jet (Fig. 6b) has an increasing divergence pattern relative to the steady jet (Fig. 5); hence, the ageostrophic circulations are enhanced, tending to drive the jet downstream, that is, to counteract the prescribed retrogression.

In the cases of the intensifying and weakening straight jets, the frontogenetic aspect of the geostrophic and ageostrophic winds are as follows. The geostrophic advection causes the isotherms to converge in the confluence (entrance) region and to diverge at the diffluence (exit) region (see KS86). In steady state these tendencies are exactly balanced by the ageostrophic circulations in both regions. Consider first the intensifying jet; Figure 6c shows that the divergence centers increase at the entrance region and decrease at the exit region relative to the steady jet (Fig. 5). Therefore, the ageostrophic circulation dominates at the entrance region, implying that frontolysis is taking place there, while the geostrophic advection dominates at the exit region, implying that frontolysis exists there, too. Hence, in this case both dynamic feedbacks have a frontolytic effect

throughout the entire jet. Thermal balance implies, then, that this tendency inhibits the prescribed intensification of the jet. The same considerations, when applied to the weakening jet, imply that frontogenesis dominates throughout the entire jet, tending to enhance the wind speed there and thus to inhibit its prescribed weakening.

c. Curved jets

In the case of a general curved jet (represented, e.g., by a baroclinic Rossby wave) the movement relative the prevailing westerlies is directed to the west (PN69). For a typical baroclinic Rossby wave, the upper-level series of troughs and ridges is associated with a corresponding series of surface cyclones and anticyclones. These surface systems constitute a positive feedback (enhancing) on the upper-level wave, provided the phase shift between the surface systems and the upper-level systems is closer to an optimal value (0.25 wavelength for the Eady case and 0.15 for the Charney case; Gill 1982). These surface cyclones (anticyclones) are expected to be found right beneath the upper level's divergence (convergence) centers (via cyclogenesis), and their intensity is proportional to that of the divergence centers. In our interpretation we will refer to the location and intensity of the upper-level divergence centers as proxy for the positive feedback that maintains the jet against dissipation. An exact balance between these two mechanisms exists in the steady jet (Fig. 11), where the phase shift between the troughs and the divergence centers is 0.25 wavelength.

Comparing the case of the progressing (retrograding) jet (Figs. 12a,b) with the steady jet (Fig. 11), we see that the location of the divergence centers is the same but with a relative decrease (increase) in intensity. Thus, a propagating jet tends to weaken due to the decrease in the positive feedback, while the retrograding jet tends to intensify due to the enhancement of the positive feedback.

In the cases of intensifying and weakening jets, the analysis is somewhat complicated by the compound changes in both the phase shift and the divergence intensity relative to those in the steady jet. In our interpretation, an increase (decrease) in the divergence intensity implies a similar change in the positive feedback, provided that the phase shift is in the range of 0.15–0.25 of the wavelength. In the case of an intensifying jet, Fig. 12c shows that the phase shift is about 0.35 wavelength, out of the optimal range, implying a reduced positive feedback. The ageostrophic circulation has, therefore, a weakening effect on the prescribed intensifying jet. In the weakening jet (Fig. 12d), the phase shift is reduced to about 0.15, being within the optimal range. This change, together with the slight intensification of the divergence centers as a whole, implies an enhanced positive feedback, which has an intensifying effect on the jet. Thus, in both the two latter cases, the net effect of the phase shift is to suppress the prescribed tendency of the jet intensity.

5. Summary and conclusions

a. Results

This study attempts to evaluate the effect of time dependence on the divergence patterns associated with both straight and curved jets, as compared to the respective steady-state patterns. Our results demonstrate that in all cases, under realistic conditions (for the retrograding jets our prescribed phase speed of 15 m s^{-1} is on the extreme side of the observed range, but was chosen to be identical to the progressing case) the inclusion of certain time dependencies does not imply a violation of the divergence patterns typifying steady jets, but that their location and intensity are significantly altered. These results are summarized in Table 1.

For both straight and curved jets that propagate in the zonal direction, the divergence patterns are unaltered in shape and location relative to the steady-state counterpart, but their amplitude decreases when the jets progress and increases when they retrograde. For an intensifying straight jet, the divergence centers increase at the entrance region and weaken at the exit. In the case of a weakening straight jet the opposite change in the intensity of the divergence centers is found. For curved jets, a variation in the meandering aspect is accompanied by an increase in the divergence centers and by a shift in their location: downstream for an intensifying jet and upstream for a weakening one. For time-varying straight jets the changes with respect to the steady jet are significantly larger at the anticyclonic half, to the right of the jet axis as compared with that in the cyclonic half.

The intensity of the divergence field is assumed here to represent that of the ageostrophic circulations associated with the jet. These circulations are assumed to have a feedback effect on the evolution of the jet. The variation of the divergence intensity for each of the time-dependent cases is interpreted as a disruption of the balance that maintains the jet in steady state, and hence affects its subsequent evolution with respect to the prescribed time dependence.

For the straight-moving jet, it is shown that the changes in the intensity of the divergence centers imply an inhibition of the prescribed movement regardless of whether it is progressing or retrograding. For a straight jet with varying intensity, the feedback mechanism tends to inhibit its prescribed change, that is, weakening of the intensifying jet and intensifying of the weakening jet. These findings indicate that the straight jet is stable with respect to the above temporal changes. For the curved jet, in the case of a propagating jet, the progressing/retrograding jet is subject to a feedback that tends to weaken/intensify the wave amplitude. The feedback associated with the change in the meandering as-

pect tends to inhibit the prescribed tendency, as in the case of the straight jet.

b. Observational assessment

The above findings and hypothesis may be verified by the use of observational data. The divergence fields extracted from observed wind fields may be compared with those calculated from the analytical functions that best fit the observed geopotential field. The phase relations between the divergence patterns and the jet may be further estimated by inspecting the location of surface cyclones and anticyclones. Since a divergence center is associated with a pronounced upward motion in synoptic-scale to mesoscale (PN69), the location of the actual divergence center may also be estimated by that of maximum cloudiness.

Acknowledgments. This work owes its origin to discussions held by BZ with P. Alpert of Tel Aviv University, while he was a Ph.D. candidate there. N. Paldor acknowledges the financial support provided by the U.S.–Israel Bi-national Science Foundation via a research grant to the Hebrew University of Jerusalem. The comments of three anonymous reviewers were constructive in improving the presentation of this work.

APPENDIX A

The Divergence of the Ageostrophic Wind in a Natural Coordinate System

In this appendix we derive the divergence field of the ageostrophic wind in natural coordinates. The derivation is used to explicitly show both the time-dependent terms and the dependence on the wind speed. The divergence operator in a natural coordinate system, when applied to the ageostrophic wind V_a, yields

$$\begin{aligned}\nabla_p \cdot \mathbf{V}_a &= \left(\mathbf{t}\frac{\partial}{\partial s} + \mathbf{n}\frac{\partial}{\partial n}\right)\cdot(V_{as}\mathbf{t} + V_{an}\mathbf{n}) \\ &= \mathbf{t}\frac{\partial V_{as}}{\partial s}\cdot\mathbf{t} + \mathbf{t}V_{as}\cdot\frac{\partial \mathbf{t}}{\partial s} + \mathbf{t}\frac{\partial V_{an}}{\partial s}\cdot\mathbf{n} + \mathbf{t}V_{an}\cdot\frac{\partial \mathbf{n}}{\partial s} \\ &\quad + \mathbf{n}\frac{\partial V_{as}}{\partial n}\cdot\mathbf{t} + \mathbf{n}V_{as}\cdot\frac{\partial \mathbf{t}}{\partial n} + \mathbf{n}\frac{\partial V_{an}}{\partial n}\cdot\mathbf{n} + \mathbf{n}V_{an}\cdot\frac{\partial \mathbf{n}}{\partial n},\end{aligned} \tag{A1}$$

where s and n are the coordinates parallel and normal (to the left) to the wind direction, respectively; $\mathbf{t}$ and $\mathbf{n}$ are unit vectors in s and n directions, respectively; and V_{as} and V_{an} are the ageostrophic wind components in the s and n directions, respectively. The orthonorm of the coordinates implies

$$\mathbf{t}\cdot\mathbf{t} = \mathbf{n}\cdot\mathbf{n} = 1 \tag{A2a}$$

$$\mathbf{t}\cdot\mathbf{n} = \mathbf{n}\cdot\mathbf{t} = 0. \tag{A2b}$$

The derivative of (A2a) with respect to either s or n vanishes identically, which yields

$$\mathbf{t}\cdot\frac{\partial \mathbf{t}}{\partial s} = \mathbf{t}\cdot\frac{\partial \mathbf{t}}{\partial n} = \mathbf{n}\cdot\frac{\partial \mathbf{n}}{\partial s} = \mathbf{n}\cdot\frac{\partial \mathbf{n}}{\partial n} = 0. \tag{A3}$$

Equation (A3) implies that the differential of each unit vector is perpendicular to that vector itself. The nonzero terms in (A1) are then

$$\nabla_p \cdot \mathbf{V}_a = \frac{\partial V_{as}}{\partial s} + V_{an}\mathbf{t}\frac{\partial \mathbf{n}}{\partial s} + V_{as}\mathbf{n}\frac{\partial \mathbf{t}}{\partial n} + \frac{\partial V_{an}}{\partial n}. \tag{A4}$$

Following Dutton (1976) and Cammas and Ramond (1989),

$$\frac{\partial \mathbf{n}}{\partial s} \equiv -\mathbf{t}\frac{\partial \alpha}{\partial s} \equiv -K_s\mathbf{t}; \qquad \frac{\partial \mathbf{t}}{\partial n} = \mathbf{n}\frac{\partial \alpha}{\partial n}, \tag{A5}$$

where α is the angle between the streamline and the east direction (taken to be positive to the left), and K_s is the streamline curvature. Equation (A4) may therefore be rewritten as

$$\nabla_p \cdot \mathbf{V}_a = \frac{\partial V_{as}}{\partial s} - K_s V_{an} + V_{as}\frac{\partial \alpha}{\partial n} + \frac{\partial V_{an}}{\partial n}. \tag{A6}$$

Following Cammas and Ramond (1989), the ageostrophic wind components are expressed by the total wind speed V, its derivatives, and the streamline curvature:

$$\begin{aligned}V_{an} &= \frac{1}{f}\frac{dV}{dt} = \frac{1}{f}\left(\frac{\partial V}{\partial t} + V\frac{\partial V}{\partial s}\right); \\ V_{as} &= \frac{-1}{f}V^2K_t = \frac{-V^2}{f}\left(K_s + \frac{1}{V}\frac{\partial \alpha}{\partial t}\right).\end{aligned} \tag{A7}$$

Substituting (A7) in (A6) yields

$$\begin{aligned}\nabla_p \cdot \mathbf{V}_a &= \frac{\partial}{\partial s}\left[\frac{V^2}{f}\left(K_s + \frac{1}{V}\frac{\partial \alpha}{\partial t}\right)\right] - \frac{K_s}{f}\left(\frac{\partial V}{\partial t} + V\frac{\partial V}{\partial s}\right) \\ &\quad + \frac{V^2}{f}\left(K_s + \frac{1}{V}\frac{\partial \alpha}{\partial t}\right)\frac{\partial \alpha}{\partial n} + \frac{\partial}{\partial n}\left[\frac{1}{f}\left(\frac{\partial V}{\partial t} + V\frac{\partial V}{\partial s}\right)\right].\end{aligned} \tag{A8}$$

Expansion of (A8) in powers of the wind speed V yields

$$\begin{aligned}\nabla_p \cdot \mathbf{V}_a &= \left[\frac{-\partial}{\partial s}\left(\frac{1}{f}\right)K_s + \frac{-1}{f}\frac{\partial K_s}{\partial s} + \frac{K_s}{f}\frac{\partial \alpha}{\partial n}\right]V^2 \\ &\quad + \left[-\frac{K_s}{f}\frac{\partial V}{\partial s} - \frac{\partial}{\partial s}\left(\frac{1}{f}\right)\frac{\partial K_s}{\partial t} - \frac{1}{f}\frac{\partial K_s}{\partial t} - \frac{1}{f}\frac{\partial \alpha}{\partial t}\frac{\partial \alpha}{\partial n}\right. \\ &\quad \left. + \frac{\partial}{\partial n}\left(\frac{1}{f}\right)\frac{\partial V}{\partial s} + \frac{1}{f}\frac{\partial^2 V}{\partial n \partial s}\right]V \\ &\quad + \left[-\frac{1}{f}\frac{\partial \alpha}{\partial t}\frac{\partial V}{\partial s} + \frac{K_s}{f}\frac{\partial V}{\partial t} + \frac{\partial}{\partial n}\left(\frac{1}{f}\right)\frac{\partial V}{\partial t}\right. \\ &\quad \left. + \frac{1}{f}\frac{\partial}{\partial t}\left(\frac{\partial V}{\partial n}\right) + \frac{1}{f}\frac{\partial V}{\partial n}\frac{\partial V}{\partial s}\right].\end{aligned} \tag{A9}$$

Equation (A9) implies that all the terms in the expression for the divergence of the ageostrophic wind are proportional to a power (1 or 2) of the wind speed or its derivative so that near jets the divergence should be significant. The along-stream changes in wind speed are much smaller than the changes in the normal direction. Thus, in the case of a straight jet, where the curvature (K_s) is negligible and the normal derivative of the wind speed ($\partial V/\partial n$) vanishes at the jet axis, we expect the divergence extrema to be located at the periphery of the jet. In the case of a curved jet where the curvature is significant, the first terms, proprtional to V^2, dominate the divergence at the jet axis. These qualitative conclusions are commensurate with observations and support our calculated fields.

In addition, the time dependence appears in 7 (out of 14) terms in Eq. (A9) and these terms are all linear with V or its derivative. This linear-only dependence on wind speed of the time-dependent terms might be the reason why calculations based on steady-state assumptions provide such a reasonable approximation to the general case.

APPENDIX B

Analysis of the Divergence Field of the Straight Jet through the Vorticity Equation

The interpretation of the calculated divergence fields in the main body of this work was done employing the variations in the wind direction and intensity. An alternative approach, used widely in the literature (e.g., Holton 1992), employs the vorticity equation. In this appendix we use the latter approach to interpret our calculated divergence field for the steady straight jet and compare the results with the approach of Uccellini and Kocin (1987) on the one hand and with the data analysis of Nakamura (1993) on the other.

Adopting the common approximations for synoptic-scale systems (e.g., Holton 1992), keeping only the horizontal vorticity advection terms and the stretching term, the divergence may be related to the vorticity by

$$\nabla \cdot \mathbf{V} \cong \frac{-1}{f + \zeta}\left[u\frac{\partial \zeta}{\partial x} + v\frac{\partial (f + \zeta)}{\partial y}\right], \qquad \text{(B1)}$$

where ζ is the relative vorticity. The discussion below follows Nakamura (1993), who analyzed the average wind field of the winter Asian jet and differentiated between the contributions to the vorticity advection due to the geostrophic and ageostrophic winds, that is,

$$\nabla \cdot \mathbf{V} \cong \frac{-1}{f + \zeta}\left\{\left[u_g\frac{\partial \zeta}{\partial x} + v_g\frac{\partial (f + \zeta)}{\partial y}\right] + \left[u_a\frac{\partial \zeta}{\partial x} + v_a\frac{\partial (f + \zeta)}{\partial y}\right]\right\}. \qquad \text{(B2)}$$

The field of absolute vorticity for the steady jet discussed in section 2 (Fig. B1) is similar to that of both Uccellini and Kocin (1987) and the observations on the Asian jet reported in Nakamura (1993). All are characterized by a pronounced south–north gradient and two extrema along the jet: a maximum to the north and a minimum to the south.

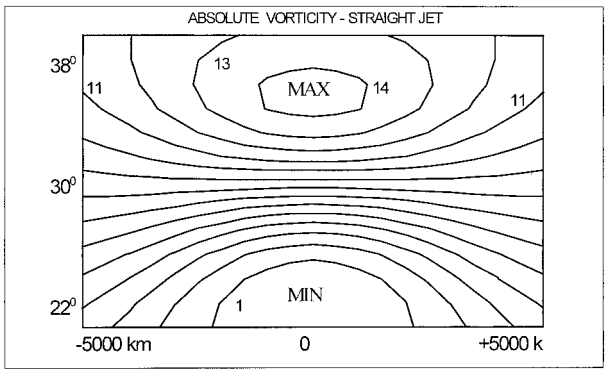

FIG. B1. Absolute vorticity field (units of 10^{-5} s^{-1}) for the steady jet discussed in section 2.

Figures B2a–c show the contributions to the vorticity advection by the geostrophic, the ageostrophic (excluding the contribution of u_a), and the total wind, respectively, for the steady jet shown in Figs. 3, 4, and 5. The geostrophic contribution to the advection of vorticity yields the familiar quadrupole pattern, in agreement with Uccellini and Kocin (our Fig. 2). The characteristic meridional ageostrophic wind pattern shown in Fig. 4 implies a negative advection along the entrance region and a positive advection along the exit region, which result in a typical dipole structure, that is, convergence at the former region and divergence at the latter region, as is shown in both Fig. B2b here and in Nakamura (1993).

The respective divergence fields are consistent with Nakamura's results in their gross features, but the quadrupole in our study is slightly more pronounced than that reported by Nakamura. The two fields differ in the relation between the magnitudes of the ageostrophic and geostrophic contributions to the vorticity advection. In the present study the magnitudes are similar, whereas in the analysis of Nakamura the contribution of the ageostrophic wind is about twice that of the geostrophic one, in agreement with Nakamura's directly calculated divergence fields.

This difference in the relative contribution of the two winds is related to the difference between the structure of the jet studied here as compared with that of Nakamura (1993). The two do not differ significantly in the magnitude of the dominant wind components, that is, u_g and v_a, but the zonal scale in the Asian jet is twice that assumed here. The effect of this difference may be evaluated by a scale analysis as follows.

Since the advection of planetary vorticity is negligible compared with that of the relative vorticity (which can be deduced from Fig. B1), the absolute vorticity is re-

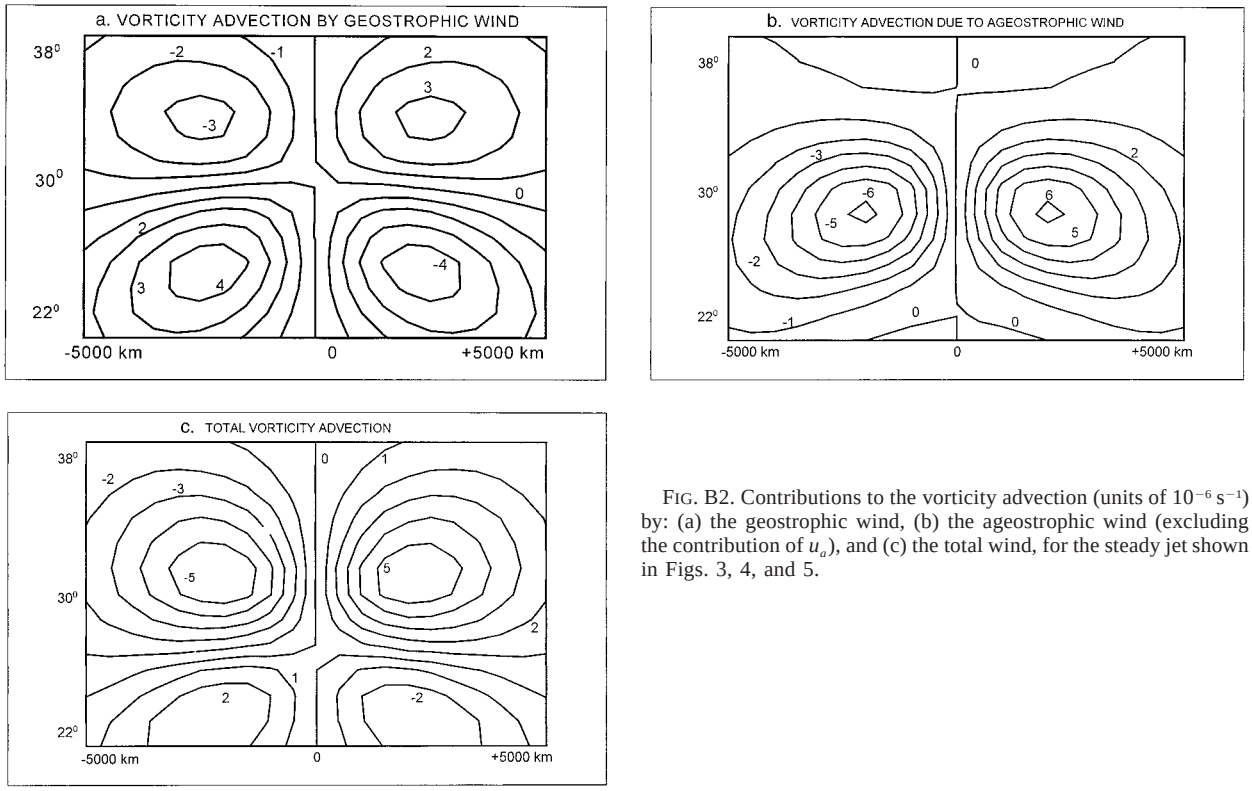

FIG. B2. Contributions to the vorticity advection (units of 10^{-6} s^{-1}) by: (a) the geostrophic wind, (b) the ageostrophic wind (excluding the contribution of u_a), and (c) the total wind, for the steady jet shown in Figs. 3, 4, and 5.

placed by the relative vorticity in Eq. (B2). The relative vorticity can be approximated by $\partial u/\partial y$, the characteristic value of which is $U\Delta_u/\Delta y$, where Δ_u is the relative variation of u_g. The respective values for Δ_u and U are ½ and 50 m s^{-1}, so the magnitudes of the two competing contributions may be approximated by

$$[\mathbf{V}_g \cdot \nabla\zeta] \cong \left[u_g \frac{\partial \zeta_g}{\partial x}\right] \cong \frac{U}{\Delta x}\frac{U\Delta_u}{\Delta y};$$

$$[\mathbf{V}_a \cdot \nabla\zeta] \cong \left[v_a \frac{\partial \zeta_g}{\partial y}\right] \cong \frac{[v_a]}{\Delta y}\frac{U\Delta_u}{\Delta y}. \qquad \text{(B3)}$$

The ratio between the magnitudes of the two contributions is then

$$\frac{[\mathbf{V}_g \cdot \nabla\zeta]}{[\mathbf{V}_a \cdot \nabla\zeta]} \cong \frac{U}{[v_a]}\frac{\Delta y}{\Delta x}. \qquad \text{(B4)}$$

Equation (B4) implies that the factors that determine the ratio between the contributions to the vorticity advection of the geostrophic and ageostrophic winds are determined by the ratio between the zonal and meridional ageostrophic winds multiplied by the aspect ratio between the length and the width of the jet.

This discussion, along with the examples mentioned above, leads to the conclusion that in straight jets the dipole structure should dominate the divergence field on the global scale, whereas the quadrupole structure dominates on the synoptic one.

APPENDIX C

Relative Contribution of Two Sinusoidal Functions with 90° Phase Relation

The divergence patterns associated with a curved jet with a time-varying meandering aspect are larger in magnitude compared with a steady-state jet whether it is amplifying or weakening. Here it is shown that this is the result of the additional contribution due to the third term in (15) over that of the first term (steady-state case).

The approximated divergence equation [(15)] for the steady state DIV_{ss} may be represented symbolically by the expression

$$\mathrm{DIV}_{ss} = A\cos\theta, \qquad \text{(C1)}$$

where θ is the phase of the traveling wave and A is some constant [that differs from that appearing in Eq. (15)]. The divergence of a time-varying meandering aspect DIV_{tv} is

$$\mathrm{DIV}_{tv} = A(\cos\theta + B\sin\theta), \qquad \text{(C2)}$$

The respective magnitude of the divergence patterns can be estimated by considering the integral of the square of the divergence field, E, averaged over one wavelength, that is,

$$E = \frac{1}{2\pi}\int_0^{2\pi} \mathrm{DIV}(\theta)^2\, d\theta. \qquad \text{(C3)}$$

The respective values for the steady-state case E_{ss} and E_{tv} are

$$E_{ss} = \frac{1}{2\pi}\int_0^{2\pi} (A^2 \cos^2\theta)\, d\theta = \frac{1}{2}A^2 \tag{C4a}$$

$$E_{tv} = \frac{1}{2\pi}\int_0^{2\pi} A^2(\cos\theta + B\sin\theta)^2\, d\theta$$

$$= A^2\left[\frac{1}{2}(1 + B^2)\right] + 2A^2B\int_0^{2\pi} \sin\theta\cos\theta\, d\theta. \tag{C4b}$$

From trigonometric identities, the last integrand in (C4b) can be rewritten as

$$\int_0^{2\pi} \sin 2\theta\, d\theta = 0. \tag{C5}$$

Equations (C4) and (C5) imply that the energy of the divergence field of a time-varying meandering aspect is larger by factor of $(1 + B^2)$ compared with that of the steady-state case, independently of the sign of B; that is, it is independent of whether the wave is amplifying or weakening.

REFERENCES

Bjerknes, J., 1951: Extratropical cyclones. *Compendium of Meteorology,* T. F. Malone, Ed., Amer. Meteor. Soc., 577–598.

——, and J. Holmboe, 1944: On the theory of cyclones. *J. Meteor.*, **1,** 1–22.

Cammas, J. P., and D. Ramond, 1989: Analysis and diagnosis of the composition of ageostrophic circulations in jet-front systems. *Mon. Wea. Rev.,* **117,** 2447–2462.

Dutkiewicz, S., and N. Paldor, 1994: On the mixing enhancement in a meandering jet due to the interaction with an eddy. *J. Phys. Oceanog.*, **24,** 2418–2423.

Dutton, J. A., 1976: *The Ceaseless Wind, An Introduction to the Theory of Atmospheric Motion.* McGraw-Hill, 579 pp.

Gill, A. E., 1982: *Atmosphere-Ocean Dynamics.* Academic Press, 662 pp.

Holton, J. R., 1992: *An Introduction to Dynamic Meteorology.* 2d ed. Academic Press, 507 pp.

Keyser, D., and M. A. Shapiro, 1986: A review of the structure and dynamics of upper-level frontal zones. *Mon. Wea. Rev.,* **114,** 452–499.

Nakamura, H., 1993: Horizontal divergence associated with zonally isolated jet streams. *J. Atmos. Sci.,* **50,** 2310–2313.

Newton, C. W., and A. Trevisan, 1984: Clinogenesis and frontogenesis in jet stream waves. Part I: Analytical relations to wave structure. *J. Atmos. Sci.,* **41,** 2717–2734.

Palmen, E., and C. Newton, 1969: *Atmospheric Circulation Systems.* Academic Press, 603 pp.

Peng, S., and R. T. Williams, 1986: Spatial instability of the barotropic jet with slow streamwise variation. *J. Atmos. Sci.,* **43,** 2430–2442.

Shapiro, M. A., and P. J. Kennedy, 1981: Research aircraft instruments of jet stream geostrophic and ageostrophic winds. *J. Atmos. Sci.,* **38,** 2642–2652.

Uccellini, L. W., and P. J. Kocin, 1987: The interaction of jet streak circulations during heavy snow events along the east coast of United States. *Wea. Forecasting,* **2,** 289–308.

——, D. Keyser, K. F. Brill, and C. H. Wash, 1985: The President's Day cyclone of 18–19 February 1979: Influence of upstream trough amplification and associated tropopause folding on rapid cyclogenesis. *Mon. Wea. Rev.,* **113,** 962–988.